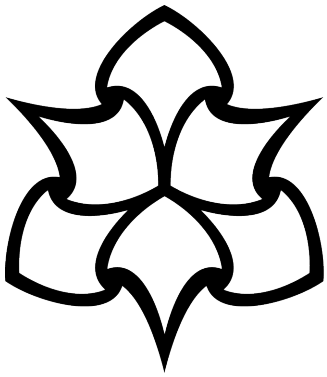

Tribological performance of graphite-like carbon films with varied thickness

Xiangru Shi[a, b], Tomasz W. Liskiewicz[b*], Ben D. Beake[c], Jian Chen[a*], Chun Wang[b]

a. School of Materials Science and Engineering, Jiangsu Key Laboratory for Advanced Metallic Materials, Southeast University, Nanjing 211189, China

b. Institute of Functional Surface, School of Mechanical Engineering, University of Leeds, Leeds LS29JT, United Kingdom

c. Micro Materials Ltd., Willow House, Yale Business Village, Ellice Way, Wrexham, LL13 7YL, United Kingdom

* Corresponding author. Tel: +86 25 52090688. E-mail address: j.chen@seu.edu.cn (Jian Chen), T.Liskiewicz@leeds.ac.uk (Tomasz W. Liskiewicz)

Abstract

Graphite-like carbon (GLC) films with different thickness were deposited on 316L stainless steel using closed field unbalanced magnetron sputtering system to investigate the influence of film thickness on the microstructure, mechanical and tribological properties. The results showed that the surface of the deposited films exhibits granular-like morphology, the sp^2 content, surface roughness increase with the increase of film thickness, leading to the lower of hardness and higher of the internal stress. Both of the of friction curves obtained by nano-tribological tests and fretting wear experiments revealed a three-stage evolution tendency with the same wear mechanism for the first two stages. The intermediate thickness GLC film had the lowest specific wear rate, whilst the fretting fatigue life increased with film thickness.

Keywords: GLC, film thickness, nano-tribological tests, fretting wear

1.Introduction

Graphite-like carbon (GLC) films are one kind of amorphous carbon films, consisting of significant sp^2 bond structure cross-linked by a small amount of sp^3 bonds [1]. Due to their unique structure, GLC films exhibit favorable properties such as high hardness (*H*), low friction coefficient (CoF), exceptional wear resistance, high optical transparency, desirable chemical inertness and bio-comparability [1-4], thus leading to widespread applications in optics, mechanical engineering and materials science, and also showing a great prospect in the field of aerospace as a new generation of solid lubrication films [5-8].

In recent years, GLC films deposited on different substrates by various techniques have been widely investigated, revealing a striking difference in their mechanical and tribological properties [2, 9-12]. One of the reasons could be attributed to the diversity of the internal structure of GLC samples, where the sp^3 hybrid carbon atoms were commonly considered to be responsible for the high hardness and the rich sp^2 bond structure were reported to demonstrate an excellent wear resistance [13]. Deposition parameters such as target currents [10], substrate bias [14, 15] and power densities [9, 15, 16], are the most common adjustable variables used to optimize the structure and properties of amorphous carbon films. For example, Wang *et al*. [10] reported that the relative content of sp^2 and sp^3 hybridisation (I_D/I_G) changed from 1.5 to 3.0 with the increase of target current from 0.4 A to 2.0 A, while the hardness and film compactness decreased. They proposed the microstructure and mechanical property evolutions resulted in the different tribological performances of the as-deposited GLC films.

Nevertheless, it is well known that deposition time is also a vital parameter to adjust the film thickness for the different requirements in applications, which also has an important influence on the structure and properties of the films. Many researchers have focused their interests on the mechanical property evolutions of amorphous carbon films with different thickness in past years [17-19]. In general, the film thickness has been found to affect not only the load capacity of the film/substrate, but also the intrinsic hardness of the films due to their characteristic growth mechanism. Manoharan *et al.* [17] revealed that the Young's modulus, fracture stress and strain values of ultra-thin glassy carbon films (4-6 nm) are far higher than those of bulk scale amorphous carbon films. Wei *et al*. [18] reported that as the film thickness increases, the I_D/I_G rate increases and the *H* decreases for the diamond-like carbon (DLC) films deposited on the silicon substrate. Bernoulli and Wyss [19] concluded that the indentation damage behavior and final morphology of DLC films deposited on ductile Ti substrate are strongly dependent on the film thickness, since thicker films shield plastic deformation of the substrate, while thinner films show increased fracture strength. For the tribological performances, Lee *et al* [20] reported that the friction coefficient of CN_x films decreased with increasing thickness for thinner film, but hardly decreased for relatively thick films.

Wang *et al.* [21] showed that the coating thickness of carbon nitride film had some effects on the surface damage during sliding contact. Although, there is still lack of systematic research on the mechanical and tribological properties of GLC films with different thickness.

Except for the internal structure, the mechanical and tribological properties of the GLC films are also dependent on the contact environment [9, 22-24]. Contact stress is an important factor influencing the friction coefficient and wear rate of GLC films. Field et al. [2] found that the friction coefficient of both of DLC and GLC films decreased with increasing normal load. They also deduced that the contact temperature between the ball and coating increased with the normal load, promoting formation of graphite-like lubricous layers. However, most of the fretting and wear experiments were conducted under relative higher contact pressure, which maybe cause the deformation of substrate, so it is necessary to explore the tribological performances of GLC films under lower contact pressure. Furthermore, compared to the usual sliding friction experiments, fretting wear is a specific damage mechanism causing failures in various components as a result of wear generated by small relative oscillation motion between two contacting surfaces under cyclic stress loading. Amanov et al. [25] used a ball-on-disc fretting tester to study fretting wear and fracture behavior of Cr-doped and none-doped DLC films deposited on Ti6Al4V alloy. They found Cr-doped DLC films fractured quickly, while none-doped DLC films showed durability over 200,000 fretting cycles. Du and his co-workers [26] investigated the fretting wear and fretting fatigue behaviors of DLC and GLC films deposited on the Titanium alloy. They indicated the fretting wear and fatigue resistance of DLC films was better than that of GLC films due to its' more excellent bonding strength and toughness. Although, to our knowledge, there is still lack of data on the comparison of sliding wear and fretting wear behaviors of sp^2-riched GLC films under dry condition. Thus, to better design those coatings for various challenging applications, a systematic research should be applied investigating the mechanical and tribological properties of GLC films.

In this work, GLC films with different thickness were deposited using closed field unbalanced magnetron sputtering technique. The microstructure and mechanical properties of GLC films were comparatively investigated as the function of film thickness. The tribological behavior of GLC films was studied in two contact modes by using the nano-tribometer and fretting wear tests under a range of normal loads. The relationship between the coatings microstructure, mechanical and tribological properties was discussed and the wear mechanism of GLC films was explored by Raman spectrum analysis.

2. Experimental details

2.1 Film preparation

Ti-containing GLC films were deposited by closed field unbalanced magnetron sputtering system (UDP-650/4, Teer Coating Ltd., UK), which was equipped with two Ti targets (purity 99.99%) and two graphite targets (purity 99.99%) opposing each other. A three-axis substrate rotation worktable was employed during the deposition process to produce uniform films. Silicon (100) wafers and mirror-polished 316L stainless steel coupons (20 x 20 x 0.5 mm) were cleaned ultrasonically in acetone for 20 min, then in ethanol for 15 min, and finally blow-dried by nitrogen gas. Coated silicon wafers were used to characterize microstructure and chemical composition of films, while the mechanical and tribological tests were conducted on coated stainless steel samples.

Prior to deposition, argon gas with a constant flow 25 sccm was introduced to the chamber and the vacuum pressure was adjusted to set at 0.3 Pa. The substrates were sputter-cleaned with Ar^+ bombardment at a bias of -500 V to remove surface oxides layer firstly, following target-cleaning for 5 min under a bias of -120 V. After that, a Ti sub-layer was deposited for 15 min at a bias voltage of -60 V to improve the interfacial bonding. Subsequently, the Ti target currents was decreased gradually to 0.8A within 45 min, while the graphite target currents were increased gradually to 3A, in order to generate a Ti-C gradient layer. Finally, uniform Ti-containing GLC films with different thickness were deposited continuously for 0.5 h, 1 h and 2 h, respectively. The detailed deposition parameters are summarised in Table 1.

Table 1. Deposition parameters of GLC films.

Process	Substrate clean	Target clean	Adhesive layer	Transition layer	GLC film
Time (min)	30	5	15	45	30 60 120
Substrate bias (V)	-500	-120	-60	-60	-60
Ti target current (A)	0.5	2	3	3-0.8	0.8
C target current (A)	0	0	0.3	0.3-3	3
Vacuum degree (Pa)	0.3	0.3	0.3	0.3	0.3

2.2 General characterisation

Surface and cross-sectional morphologies of GLC films were examined using scanning

electron microscopy (SEM) (XL-30, FEI Co., USA) at 20.0 KV. Film thickness was measured from SEM cross-sections and the deposition rate was calculated based on the total deposition time. The surface roughness was determined by atomic force microscopy (AFM) (Bruker Co., German). X-ray diffraction (XRD) was carried out by a X-ray spectrometer (D8-Discover, Bruker Co., German) with Cu Kα radiation (λ=1.5405 Å). Raman spectra in the range of 1000-2000 cm^{-1} were obtained to investigate the bonding of GLC films by a Raman spectrometer (inVia-reflex, Renishaw Co., UK) using an Ar^{+} laser of 532 nm.

2.3 Mechanical properties

Hardness (*H*) and elastic modulus (*E*) of GLC films were measured using a calibrated nanoindentation system (NanoTest Vantage, Micro Materials Limited, UK) with a Berkovich diamond indenter by applying the Oliver-Pharr analysis [27]. In order to clarify the substrate effect, a range of indentation loads from 2 to 50 mN was used. Fifteen repeats were carried out on each sample at each load. The elastic modulus E here is determined from the slope of the unloading force-displacement curve via the relations below:

$$\frac{1}{E_r} = \frac{1-\nu^2}{E} + \frac{1-\nu_i^2}{E_i} \quad (1)$$

Where E_r is the reduced modulus, E and ν (0.22) [28] are Young's modulus and Poisson's ratio for the films, E_i (1140GPa) and ν_i (0.07) are the same quantities for the diamond indenter [27].

To calculate the internal stresses in films, the curvature radius was measured by Talysurf surface profilometer and the level of stress was established using Stoney's equation [29]. The adhesion strength between the substrate and film was measured by a scratch test system (WS-2002 equipped with an acoustic emission detector). In a typical testing, a diamond pyramidal tip was driven across the film surface and loaded at the rate of 60 N/min to the peak load 60 N. The maximum trace length was 4 mm, and the critical load was defined at the point where an abrupt increase was observed in the acoustic signal. Rockwell indentation system (HR-150A) was also used to evaluate the adhesion of the films by keeping the indenter (cone angle 120◦, tip radius 0.2 mm) in contact with the sample at a given maximum load of 150 kgf for 40s.

2.4 Tribological testing

Nanotribological experiments were performed using a reciprocating type pin-on-disc nanotribometer (NTR^3, Anton Parr) at four normal loads: 200, 500, 800 and 1000 mN. Si_3N_4 ceramic balls with a diameter of 4 mm were used as the counterparts. Friction

tests were conducted under room temperature with the relative humidity of approximately 40 %, and the stroke length and sliding frequency were set at 500 μm and 5 Hz, respectively. In order to obtain a statistically valid data, three repeated tests with 50,000 cycles for each load were carried out at different position on each sample.

Fretting wear was carried out using fretting device with a dedicated electrodynamic shaker as reported in [30-32]. All experiments were conducted in dry conditions at 5Hz frequency and ±100 μm displacement amplitude. The counter-body in fretting test was 25 mm diameter Si_3N_4 ceramic ball. The normal loads applied were in the range of 10-40 N, and they were set to generate a corresponding maximum contact pressure to that applied in the nano-tribological tests (as shown in Table 2). Fretting wear film durability was defined as the point where the friction coefficient increased sharply to the value of the stainless steel substrate.

After tribological tests, worn surfaces and counterpart balls were characterised by optical microscopy and white light interferometer (NPFLEX 3D, Bruker). The wear tracks were analysed by Raman spectroscopy.

Table 2. Normal loads and corresponding contact pressures for the nanotribological and fretting experiments.

Nanotribometer testing		Fretting wear	
Normal load (N)	Contact pressure (GPa)	Normal load (N)	Contact pressure (GPa)
0.2	0.46	10	0.49
0.5	0.62	20	0.62
0.8	0.72	30	0.71
1	0.78	40	0.78

3. Results

3.1. Microstructure and morphology of GLC films

The cross-sectional and surface morphologies of GLC films with different deposition time are compared in Figure 1. The enlarged cross-sectional morphology in junction with composition analysis is presented in Figure S1. All these films show clear characteristic tri-layered structure: a smooth and dense Ti base layer on the Si substrate, a gradient layer, and a uniform and compact top layer with a columnar structure. The thickness of Ti base layer in cross-sectional images of Figure 1 is almost constant for all the samples, which confirms the stability of the sputtering system. The total film thickness increases with the increase of the deposition time. By measuring the thickness

of different layers as listed in Table 3, it can be found that the deposition rate for the top layer increases significantly from 5.0 to 11.7 nm/min with the deposition time extend from 0.5h to 1h, while the data is close for 1h and 2h samples.

Table 3. The calculated top layer thickness and corresponding deposition rate for GLC films deposited with different sputtering time.

Samples	Film thickness (nm)			Deposition
	Total thickness	Bottom two layers	GLC top layer	rate (nm/min)
0.5h	550	400	150	5.0
1h	1100	400	700	11.7
2h	1520	400	1120	9.3

As shown in the SEM cross-sections in Figure 1, the microstructure of 0.5h and 1h GLC samples is more uniform and compact, while the columnar structure is more developed for the 2h sample. In addition, the surface morphologies show a fine grain structure which coarsens with increasing deposition time. A looser structure with more defects is observed for 2h GLC sample in comparison to the dense and smooth surface for 0.5h sample. Such morphological evolution was also confirmed by AFM in Figure 1. The surface roughness (R_a) was 3.7, 5.7 and 6.1 nm for 0.5h, 1h and 2h samples, respectively, consistent with the SEM results.

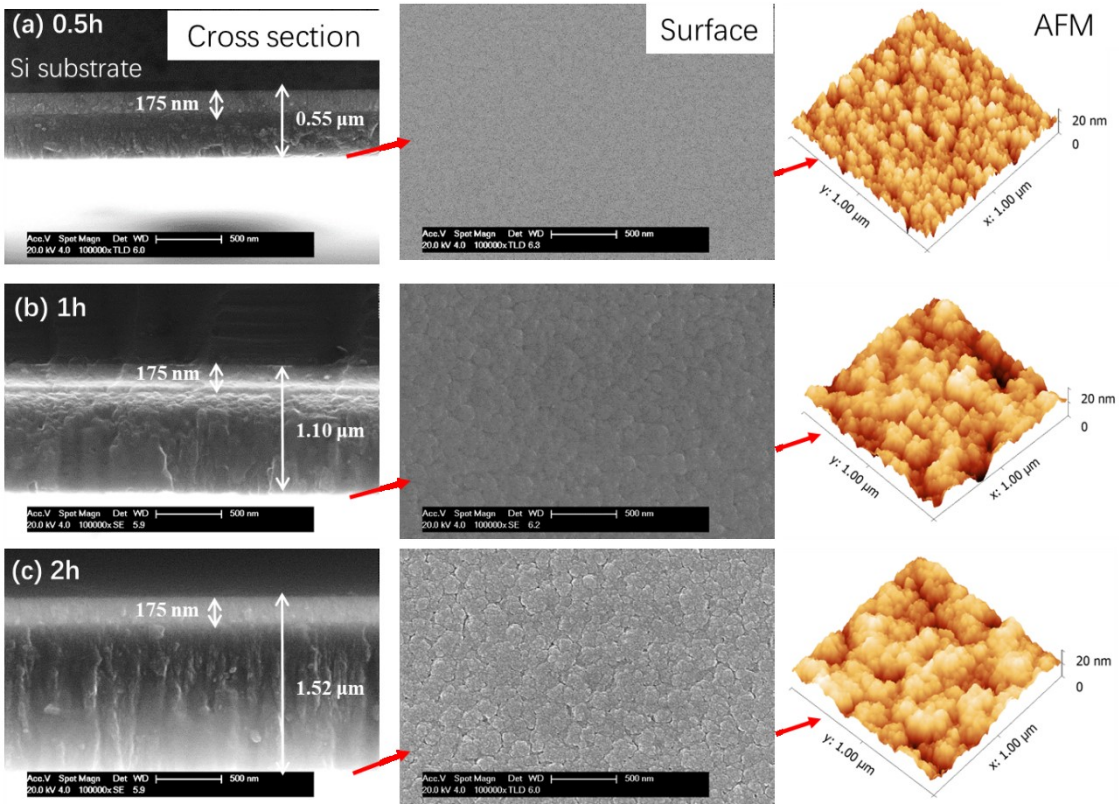

Figure 1. SEM images for cross-sectional and surface morphologies and corresponding

AFM surface images of GLC films at different sputtering time: (a) 0.5h, (b) 1h, (c) 2h.

Figure 2a shows the XRD patterns of the GLC films. All the films exhibit broad scattering peaks from 10° to 30°, verifying their amorphous structures [33]. Raman spectra of GLC films are shown in Figure 2b. Two characteristic peaks (as called G peak and D peak) [34-36] are dominated for the GLC films, which lie at ~1560 cm^{-1} and 1360 cm^{-1}, respectively. The G peak is caused by the bond stretching vibration of all pair of sp^2 atoms in both rings and chains, while the D peak is the breathing mode of those sp^2 sites only in rings but not in chains [36, 37]. It is found that the intensity of D peak (I_D) of GLC film increases gradually with the extension of deposition time, which is usually considered as the sign of increasing sp^2 sites, due to the diversity of resonances of D (disorder) and G (graphitic) bands [38].

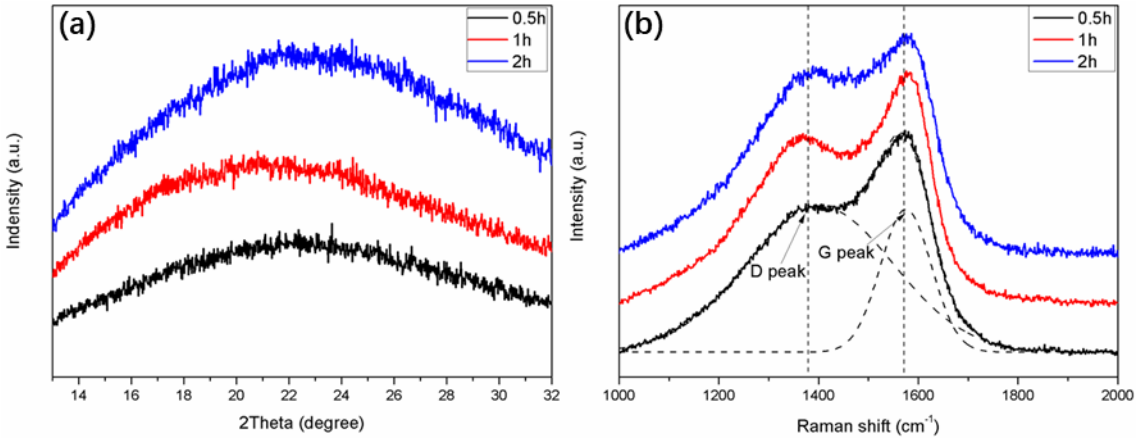

Figure 2. (a) XRD images and (b) Raman spectrum of GLC films at different sputtering time.

More detailed information can be obtained after Gaussian fitting of the two characteristic peaks. As shown in Figure 3, the value of I_D/I_G (the area ratio of two fitted peaks) is a measure of the size of the sp^2 phase, while both the position and the full width at half maximum (FWHM) of G peak indicate the disorder of GLC films [36]. It can be seen that the I_D/I_G increases from ~2.64 to ~3.86 when the time increases from 0.5h to 2h. Meanwhile, the peak position shifts to high wavelength from 1574 cm^{-1} to 1584 cm^{-1}, and the FWHM for G peak decreases from 119 to 109 cm^{-1}. All the results indicate the increase of sp^2 sites and clustering of sp^2-hybirdized phase with the increase of deposition time. Furthermore, the structure disorder and amorphization degree of the GLC films can be explained by the FWHM of G peak, in which a broader G peak indicates more disordered sp^2 cluster [36]. In other words, the amorphization and the disorder degree of films decreases with the extension of sputtering time shown by the decreasing of FWHM of G peak and increasing of G peak position.

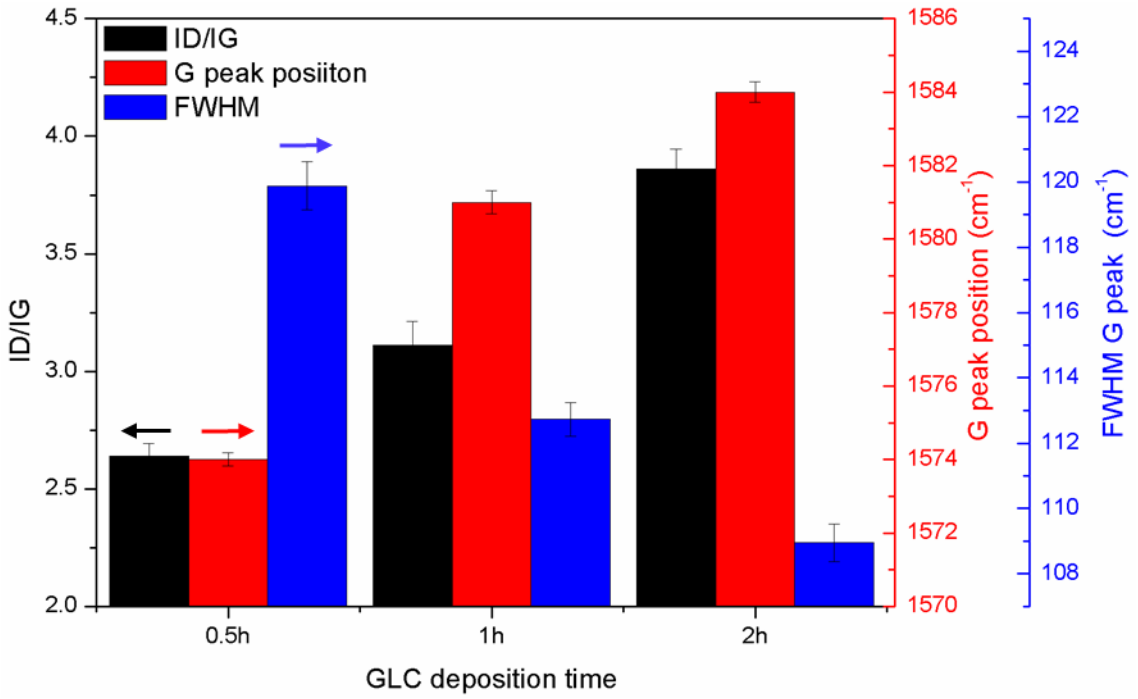

Figure 3. I_D/I_G, G peak position and the full width at half maximum of G peak of the GLC films deposited with different time.

3.2. Mechanical properties of GLC films

The mechanical properties of GLC films deposited at different time are plotted in Figure 4 (a-c) as a function of Relative Indentation Depth (RID, indentation depth/total film thickness). As seen in Figure 4 (a, b), RID has an important effect on the *H* and *E*, where the *H* gradually decreases while *E* increases slowly with the increase of RID. Among the GLC films, the GLC sample with 0.5h sputtering time possesses the highest *H* and E, while the 2h sample shows the lowest *H* value and 1h sample has the lowest *E* value. Figure 4c shows the variation in *H*/*E* with RID. *H*/*E* has been considered as an important indicator of the wear performance for hard coating materials [39, 40], since higher values can result in improved wear resistance.

Figure 4d shows the critical load and internal stress of GLC films deposited with different time. The compressive internal stress of GLC films increases from 0.32 GPa to 1.02 GPa as the sputtering time increases from 0.5h to 2h. The scratch test critical load increases from 12 N to 23 N when the sputtering time extended from 0.5h to 1h, and then slightly decreases to 17 N for 2h. The optical images of the scratch traces are shown in Figure S2(a-c). Optical micrographs of Rockwell indentation tests are also shown in Figure S2d, providing a qualitative measure of differences in adhesion strength. Apparent cracks and delamination of the films occurred around the indentation for 0.5h sample, while there was just a little chipping happened for 1h and 2h sample, especially better for the 1h sample.

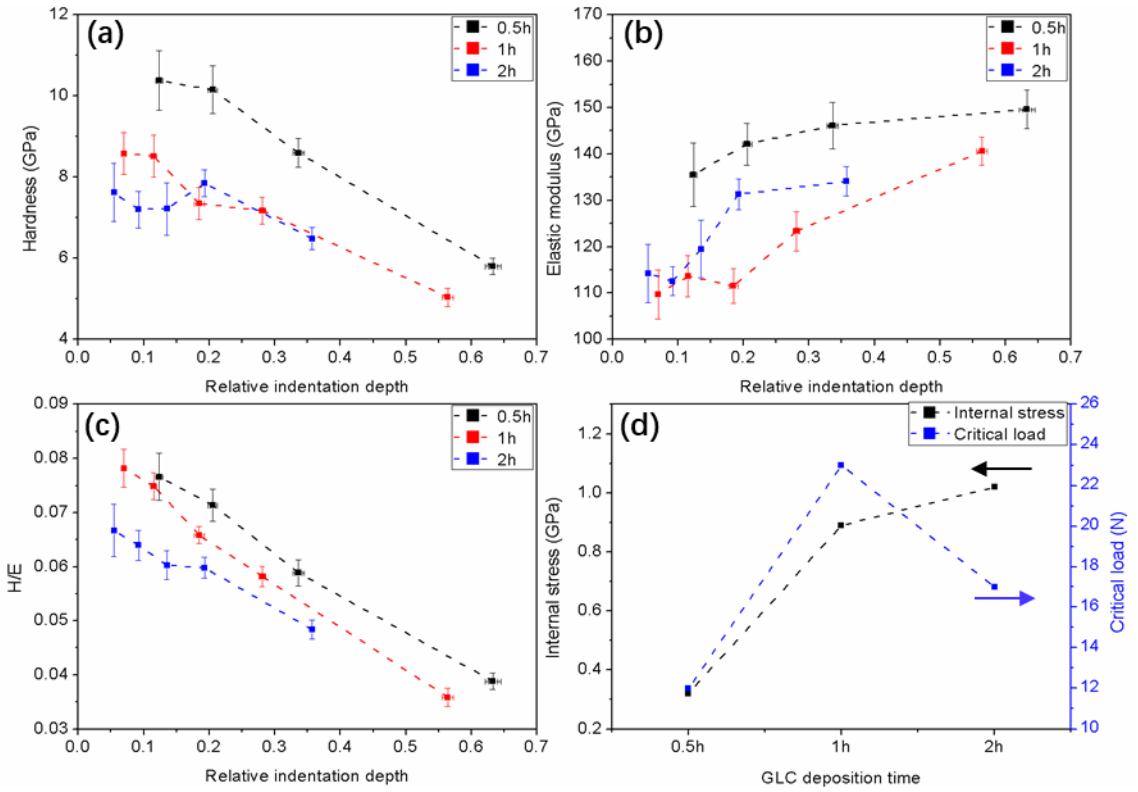

Figure 4. Mechanical properties of GLC films as a function of relative indentation depth: (a) Hardness (*H*), (b) Elastic modulus (*E*), (c) *H*/*E*, and (d) variation in internal stress and scratch test critical load with composition.

3.3. Tribological performance of GLC films

3.3.1. Friction and wear behaviours of GLC films with nano-tribometer

Typical friction coefficients of GLC films and the stainless steel substrate obtained in nano-tribological tests at a normal load of 1000 mN are shown in Figure 5a. Figure S3 shows the good repeatability of CoF curves with the same applied load of 1000mN at three different positions on 1h GLC sample. The evolution of CoF during the test follows three distinct stages as illustrated in Figure 5b. In the first stage, the CoF decreases dramatically and stabilize at ~0.1 with different time spans. As indicated by the arrows in Figure 5c, the lasting duration and corresponding stable CoF for 0.5h, 1h and 2h GLC films are ~7000, ~2000 and ~300 cycles, and 0.08, 0.09 and 0.12, respectively.

During the second stage, the CoF increase in a rough way with different rates to maximum values and then decrease gradually. Among the GLC films, the increasing rate of CoF (reflected by the curves slope before the highest value) increases apparently with the extension of sputtering time. The last stage is the stationary phase of CoF in which the CoF increases with the extension of sputtering time. Although, it can't be ignored that the CoF of 0.5h sample is a little higher than 1h sample at the end of 5000

cycles. Figure 5d shows the effects of applied normal forces on the CoF curves. It can be seen that the friction curve in the first stage is almost insensitive to the applied loads, while with the decrease of forces more cycles are needed to reach a stable coefficient in the second stage, and the stable coefficient increases in stage 3.

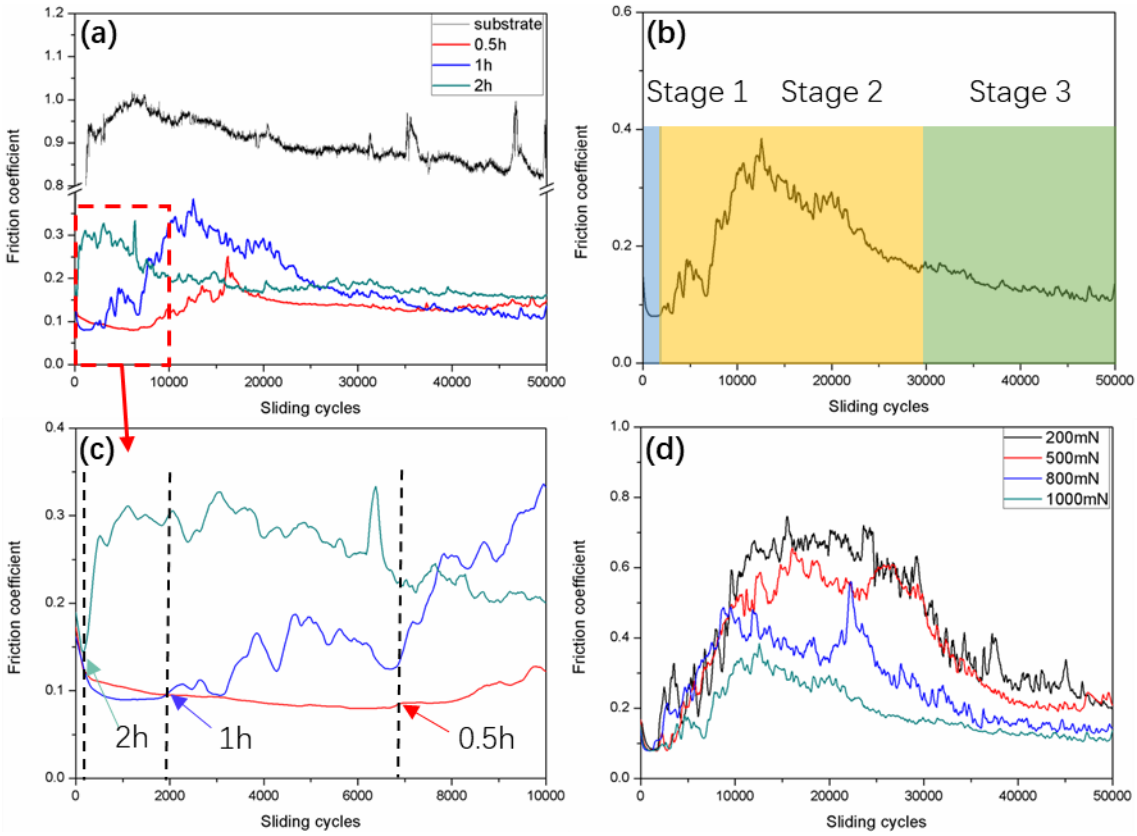

Figure 5. (a) Friction coefficient of steel substrate and the GLC films as a function of sliding cycles at a normal load of 1000mN for nanotribological tests, (b) the friction curve of 1h sample showing different stages, (c) the magnified friction curves of the first 10000 cycles from image (a) for GLC films, (d) the friction curves of 1h sample under different normal loads.

The 3D topography of wear tracks and the corresponding 2D profiles produced at 1000mN are shown in Figure 6. All the wear tracks present apparent ploughing effect, and transferred materials can be observed in the edge of the wear tracks. The width of wear tracks increases with the increasing of film thickness, while the wear depth shows a totally different tendency, which is also an important factor to the anti-wear performance of GLC films. The maximum wear depth shown in the wear profiles is about 0.8, 0.35 and 0.6 μm with the extension of sputtering time from 0.5h to 2h, respectively. The specific wear rate of GLC films at a normal load of 1000 mN are derived and shown in Figure 7a, which is 2.0, 1.5 and 2.4 x 10^{-16} m^3 N^{-1} m^{-1} for 0.5h, 1h and 2h films, respectively. Figure 7b shows the effects of normal forces on the specific wear rate, which displays a decreasing trend with the increase of forces.

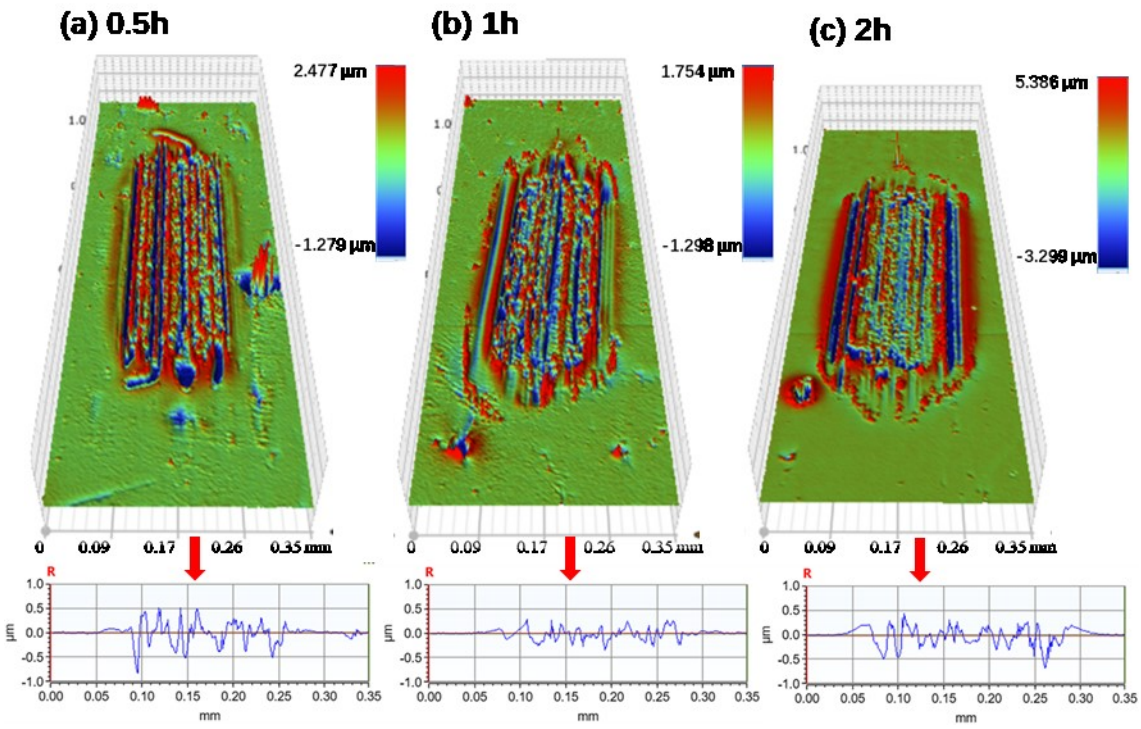

Figure 6. 3D topography of wear tracks and the corresponding two-dimensional profiles for GLC films deposited with different sputtering time at a normal of 1000 mN, (a) 0.5h, (b) 1h, (c) 2h.

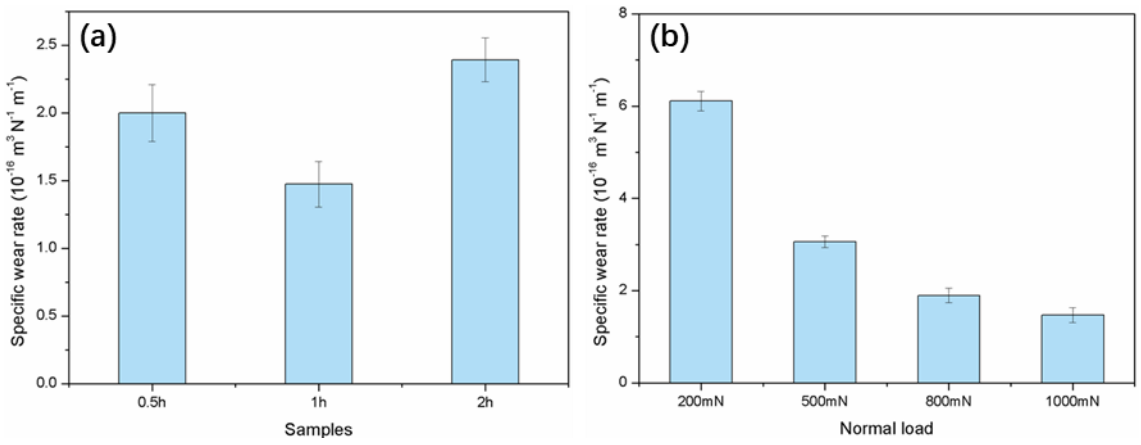

Figure 7. Specific wear rate of (a) GLC films deposited with different sputtering time at a normal load of 1000 mN, and (b) 1h sample at different normal loads.

3.3.2 Fretting tests

Depending on the contact condition, relative displacement and stress magnitude at the interface during fretting wear, partial slip or full sliding condition (gross slip) can be observed in the contact, which relate to cracking and wear damage mode, respectively [30, 41]. Figure 8a shows the typical fretting map (friction force-number of cycles-displacement amplitude, Q-D-N curve) for GLC films. All of curves present a closed

parallelogram, which indicates that fretting contact region is always in the gross slip region, and the fretting damage is mainly caused by sliding wear. Figure 8b shows the average CoF of steel substrate and GLC films as a function of fretting cycles at a normal load of 40 N under dry fretting condition. It can be seen that the uncoated substrate showed a higher CoF of about 0.9, which is almost identical to the value obtained by nanotribometer (Figure 5a).

Similarly, the fretting friction curves for GLC samples here can also be divided into three stages. As shown in Figure 8c, the CoF drops quickly to a relative stable value after running-in period in stage 1, and then increases gradually in stage 2, followed by a dramatic increase to the value of CoF of substrate in stage 3. This can be linked to failure of for the GLC films and the transition point can be regard as the fretting fatigue life. Among the GLC films, the CoF is always lower for the GLC sample with less sputtering time, while the duration of stage 1 decreases with the increase of sputtering time (marked with point 1 in Figure 8b), this result is consistent with the nano-tribological tests. The fretting fatigue life of GLC films is marked by point 2 in Figure 8b, which is about 7500, 9000 and 12000 cycles for the 0.5h, 1h and 2h GLC films, respectively, increasing with the sputtering time. The effect of normal loads on the fretting behaviour is also investigated for 1h GLC film. One can see from Figure 8d, there is a slight decrease of the CoF and shorten of the fatigue life for GLC films with the increase of normal load, which almost can be neglectful because of the experimental error.

The 3D topography of first 5000 cycles fretting wear trace and the corresponding 2D profile of wear depth for the GLC films at a normal load of 40 N are shown in Figure 9. The wear tracks present similar ploughing effect with the nano-tribological tests, which is most visible for 2h sample. However, the specific wear rate is very difficult to calculate due to the very shallow wear depth.

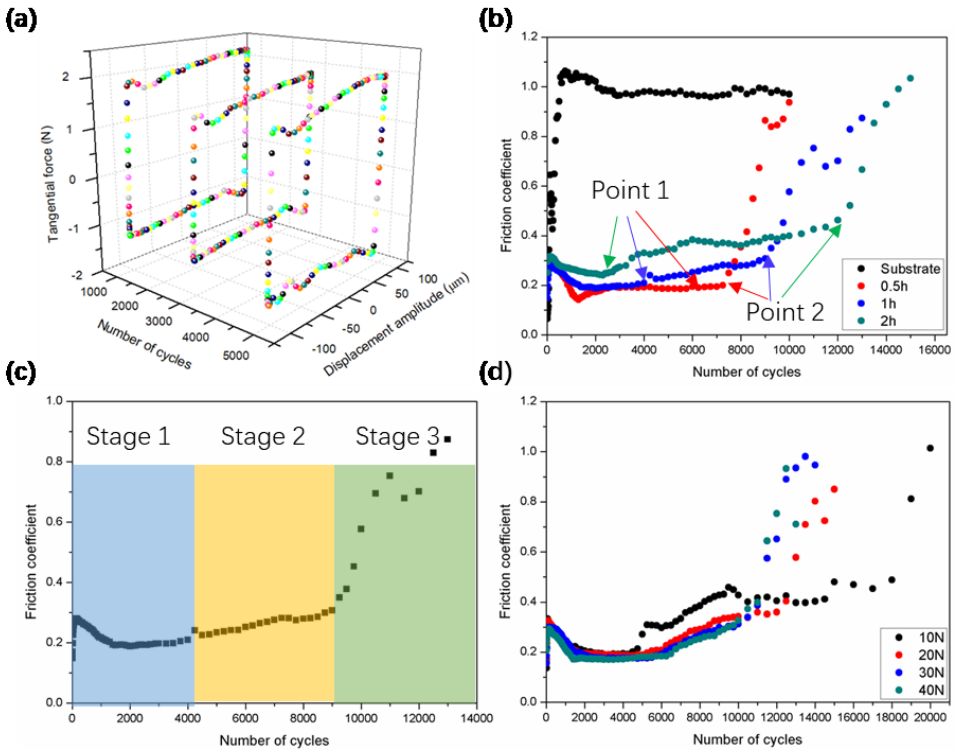

Figure 8. (a) Typical fretting log (Q-D-N curve) for 1h film, (b) friction curves of substrate and GLC films as a function of sliding cycles at a normal load of 40 N, (c) the friction curve of 1h sample showing three different stages, (d) the friction curves of 1h sample under different normal loads.

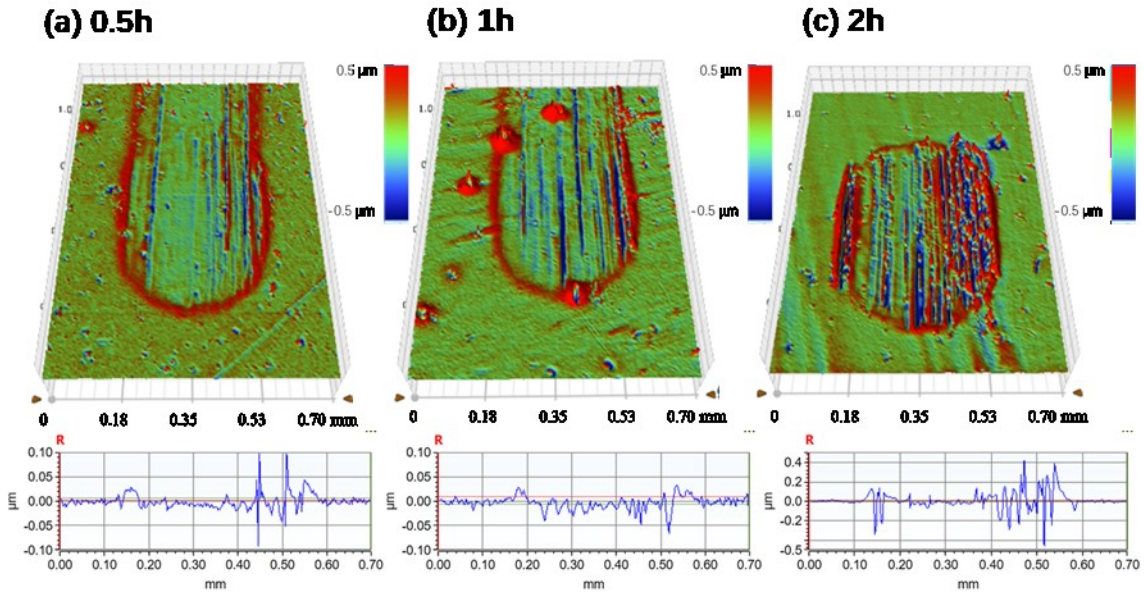

Figure 9. 3D topography of first 5000 cycles fretting wear tracks and the corresponding 2D profile of wear scars of GLC films at a normal load of 40 N, (a) 0.5h, (b) 1h, (c) 2h.

4. Discussion

4.1 The microstructure evolution of GLC films

For the magnetron sputtering system, the deposition rate and film microstructure can be significantly affected by many factors such as the incident particle energy, type of incident particle, type of target material, incident angle, and temperature in the chamber and so on [42]. Although the GLC films with different thickness were prepared by only changing the sputtering time and keeping the rest deposition parameters same in this work, the variation of deposition rate and the microstructure indicate that the growth of the films can not be regarded as a linear mode with the time. Moreover, the sp^3 fraction shows a decreasing tendency with the extension of deposition time. Such surprising results can be ascribed by that the add-up bombardment of energetic particles. According to the subplantation model [43-45], the impinging hyperthermal species with the energy beyond a critical value will have a high probability to penetrate into the top layers of bombarded sample, enter subsurface interstitial sites and increase the local density. Thus, the mobility of the deposited atoms increases with the increase of deposition time.

Although the extra energy carried by the implanted C^+ may be beneficial to the transformation from sp^2 to sp^3 at relative lower energy range, thermalization and relaxation can take place at higher energies allowing the excess density to relax to zero, and cause a loss of sp^3 bonding at higher ion energies [46]. Meanwhile, the deposition rate increased with the relaxation of the subplanted carbon atoms to the surface with the rise of the deposition time. Besides, the continuous bombardment can also cause the heating effect on the film/substrate which is beneficial to the formation of sp^2 clusters and grain coarsening, leading to the higher surface roughness [47, 48]. Chen *et al* [46] and Laugier *et al.* [49] also reported with the increase of temperature the sp^2 content in amorphous carbon films by magnetron sputtering firstly decreased and then increased when the temperature improved to a critical value. Thus, the increase of sp^2 content, grain size and surface roughness can be attributed to the synergistic effects of the higher mobility of the deposited atoms and heating effects with the extension of deposition time.

4.2 The relationship between the microstructure and mechanical properties

The hardness and elastic modulus of GLC films exhibited a strong dependence on the RID shown by Figure 4(a, b). In general, lower maximum indentation depth (<10% of the film thickness), the closer to the intrinsic hardness and elastic modulus of films [28]. At RID <0.1, the hardness of GLC films is ≈8-11 GPa, which is close to values of 7.2-11.7 GPa previously reported by unbalanced magnetron sputtering [50]. The hardness of GLC films may be explained by the microstructure model [51, 52] where graphite-

like carbon films could be composed of a strong sp^2 σ-bonded 3D carbon network cross-linked a small amount of sp^3 sites, where the sp^3 bonds act as a bridge to interconnect the adjacent graphitic planes together. The higher hardness of the thinner film here may be result from the enhanced connectivity of separated graphite cluster with more sp^3 sites. In addition, the most compact morphology for the GLC film with the sputtering time of 0.5h is another factor for the highest hardness, with the looser microstructure and greater defects in the GLC films deposited with longer time resulting in lower hardness. At higher RID, the measured hardness and modulus are increasingly dominated by the substrate (softer but stiffer than the films) causing the hardness to decrease and increase of modulus with increasing RID.

The internal stress consists of intrinsic stress and thermal stress. The thermal stress is caused by the difference of thermal expansivity between the film and the substrate, while the intrinsic stress is attributed to several factors, such as the doping of impurity, formation of defects and phase transformation. The internal stress calculated here is much lower than the conventional DLC films in literature [51]. On the one hand, the deposition of Ti adhesive layer and the Ti-C gradient layer can decrease the mismatch of crystal lattice between the film and substrate, which can decrease the internal stress. On the other hand, the lack of sp^3 content in the film also results in the lower internal stress, since the presence of sp^3 phase would strain sp^2 clusters and thus providing stress for the film. Fallon *et. al* predicted [52] that the internal stress shows an almost monotonic increasing tendency with changing sp^3 content in the films. It is interesting to note the internal stress evolution for GLC films with different thickness exhibits an inverse correlation with the sp^3 content in this research. As mentioned above, many sp^2 clusters will be trapped on the growing surface for the film with longer sputtering time, forming a loose and porous structure, which mismatch with the substrate crystal lattice and lead to the high stress. Furthermore, the higher intrinsic stress is also attributed to the accumulative effect of the flaws with the increasing of film thickness. Previous studies have shown the critical load is not only related to the mechanical strength of the film and substrate, but also depends on the hardness and internal stress of the films [54, 55]. During the indentation and scratch tests, the normal load is enough to cause the plastic deformation of films and substrate, the larger diversity of hardness between the film and substrate for 0.5h sample causes the film failure easier. The looser structure and higher internal stress explain the slight decrease of critical load for 2h sample compared to the 1h sample.

4.3 Tribological performance and wear mechanism of GLC films

To investigate the friction and wear mechanism of the GLC films under dry sliding conditions, the friction tests for 1h sample at 1000 mN normal load with different sliding cycles were conducted. Figure 10 shows the optical morphology images of the wear tracks and the mating Si_3N_4 balls, and Figure 11 exhibits the corresponding Raman

spectrum of wear tracks. When the number of sliding cycles is fewer than 2000, the friction curve shown in Figure 5b is in the range of stage 1. As can be seen in Figure 10a, the wear track of the film is very smooth in appearance and the film is still intact, while there is a little transferred material covered on the surface of the mating ball. Raman spectrum shows little change in the D peak and G peak for the worn surface after 2000 cycles, compared to the raw surface, which evidenced no change for the film structure in stage 1. All of these result in the stable and lower CoF in stage 1. In the second stage of friction curve (from 2000 to 30000 cycles), obvious abrasive wear happened in the surface. From 2000 to 15000 cycles, the width of wear trace increased gradually and the contact surface was destroyed almost totally by the cutting particles, which explained the sharply increased and fluctuant friction curve during this period. During 15000-30000 cycles, the width of wear trace is basically constant, and the wear particles were removed gradually from the wear region to the edge of the wear trace and partially stuck on the mating ball to form a dense transfer layer (shown in Figure 10d). This phenomenon led to the slow decrease of CoF to stable value. As can be seen from Raman spectrum, the D peak has a gradual increase while the G peak shift to high wavelength from 2000 to 30000 cycles, which proved the transformation of graphite-like structure during the friction tests. When the sliding cycles above 30000, a complete and compact transfer layer is formed (Figure 10 (d, e)), and the structure reflected by the Raman spectrum remains unchanged, that should be the reasons for the steady CoF in stage 3. The low CoF of GLC films in dry sliding was generally attributed to the graphite-like microstructure inside the carbon matrix and the carbonaceous transferred-layer formation on the mated surface [56, 57]. Both of them have been proved by the Raman spectrum (Figure 11) and the optical images of the Si_3N_4 ball during different wear period.

As seen from Figure 5a, the CoF increased with film thickness, though the relative content of sp^2 sites increased. This phenomenon is highly likely to be linked with the difference of mechanical properties for GLC films. Generally, the hardness of film has been often used as an important criterion to evaluate their wear resistance [58]. Leyland and Matthews [39] even established a relationship between the mechanical parameter H/E and the wear performance. It was proposed the elastic modulus and film toughness is very important during the wear process, especially for the abrasive wear. Films with high hardness are more resistant to contact stress, thus producing a smaller contact area at a certain normal load. From Figure 6, one can see that there is almost no plastic deformation for the substrate at the normal load of 1000 mN, so the intrinsic hardness of the films is dominated at the initial contact, which decreased with increasing of film thickness. In stage 1, the highest hardness and lowest surface roughness for 0.5h sample is responsible for the lowest CoF and the longest duration, while the lowest hardness and loose structure for 2h sample results in the lowest load-capability to generate phase transformation. With the extension of friction cycles, the wear particles were generated and acted as a third party to cause high local stress, which caused the occurring of phase

transformation from sp^3 to sp^2. The adhesive effects of π bonds in sp^2 structure with the mating surface is slighter than the σ bond in sp^3 carbon atoms, that promote the formation of transfer layer with low shear strength. The increasing amounts of cutting particles aggravate the abrasive wear on the film surface and increase the CoF in stage 2. The looser microstructure and more defects in the thicker films accelerate the increasing rate of CoF. The wider wear trace generated by lower hardness and *H*/*E* for thicker films shown in Figure 6 results in the increase of CoF of GLC films in stage 3.

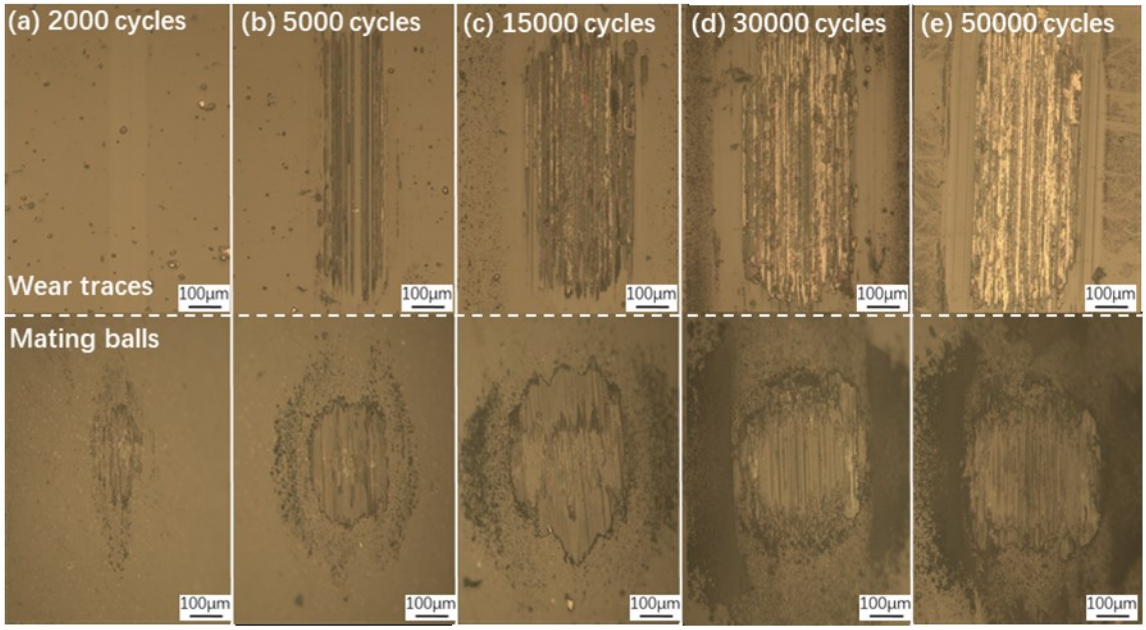

Figure 10. Optical morphology images of wear trace and mating balls for 1h sample at a normal load of 1000mN with different sliding cycles (a) 2000 cycles, (b) 5000 cycles, (c) 15000 cycles, (d) 30000 cycles, and (d) 50000 cycles.

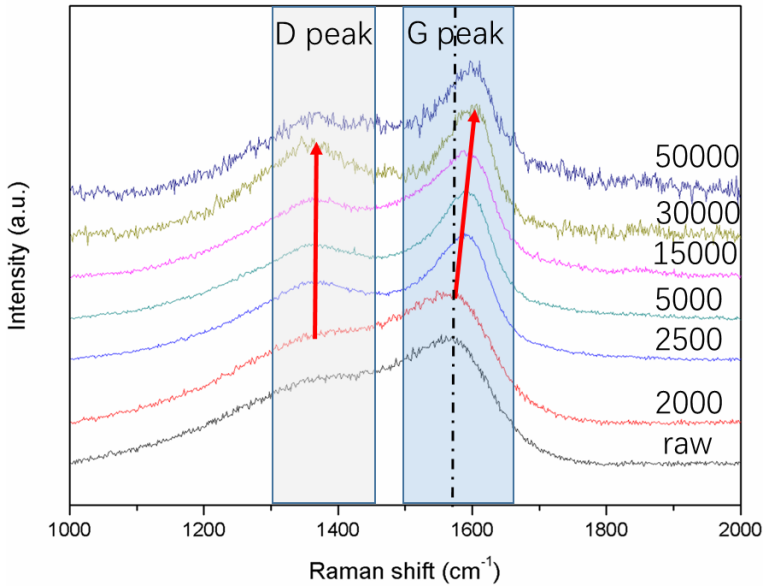

Figure 11. Raman spectra of the worn surfaces for 1h sample at a normal load of

1000 mN with different sliding cycles.

For the 0.5h sample, the maximum depth at the end of 50000 cycles is close to 0.8 μm, exceeding the total thickness of the film (0.55 μm), therefore the carbon layer had already worn out and the friction and wear happened between the substrate and the mating ball, which result in the CoF of 0.5h sample a little higher than 1h sample at the end of the test and a higher specific wear rate. The wider and deeper wear trace generated by the lower hardness and loose microstructure for the 2h film cause the higher specific wear rate than 1h GLC film. The effect of normal load on the CoF is shown in Figure 5d. The increasing of normal load may accelerate the removal of cutting particles in stage 2 and the formation of stable transfer layer in stage 3, which explains the decrease of CoF with the increase of normal load.

Figure 12 and 13 shows the worn surface of fretting tests for 1h sample at a normal load of 40 N with different fretting cycles and the corresponding Raman spectrum of the surface. As can be seen, the fretting wear mechanism of GLC films for the first two stages is similar with the nano-tribilogical tests. In stage 1 (before 4000 cycles), the surface of fretting wear trace is very smooth with some shallow scratch and the structure shown by the Raman spectrum is almost the same with the raw surface. The CoF is stable and lower after the running-in period. Phase transformation is caused by stress concentration and film surface is destroyed by shear stress in stage 2 due to the generation of abrasive particle. Although, the CoF of GLC films under fretting tests is higher than the values obtain by nano-tribological experiments, which could be caused by the larger contact area with the bigger mating balls despite the similar contact stress. In addition, the third stage for fretting test is totally different. In that case, extremely high contact stress could be generated by the abrasive particles at high 40 N normal load, which will penetrate into the substrate and destroy the films quickly, thus the CoF increases sharply to the values of substrate. The Raman spectrum at 10000 cycles detects no C elements signal, and EDX also evidenced the exposing of steel substrate. The higher CoF for the thicker GLC films is also attributed to the lower hardness and looser structure. The enhanced film thickness takes an advantage of prolonged fatigue life. Due to the enough high concentrated stress to destroy the films, the normal load has almost no effect to the CoF and fatigue life for the GLC films.

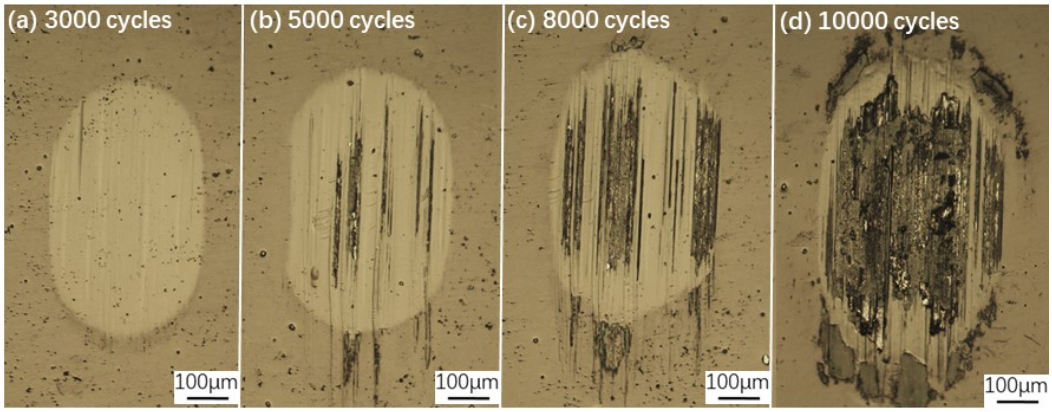

Figure 12. The optical morphology images of fretting wear trace for 1h sample at a normal load of 40 N with different fretting cycles, (a) 3000 cycles, (b) 5000 cycles, (c) 8000 cycles, and (d) 10000 cycles.

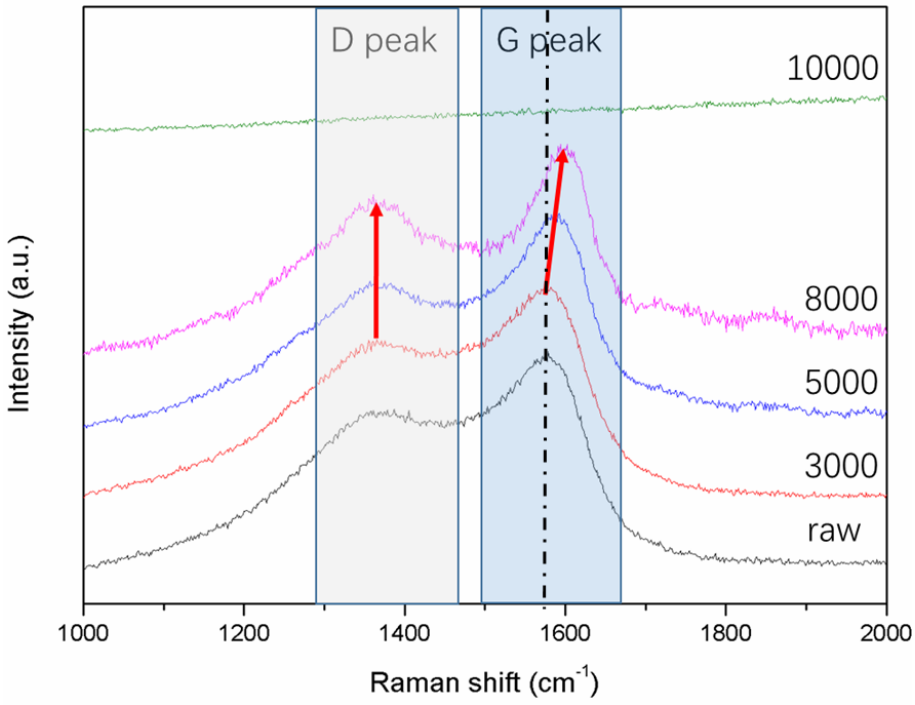

Figure 13. Raman spectra of the fretting wear surfaces for 1h sample at a normal load of 40 N with different sliding cycles.

5. Conclusion

GLC films with different thickness (0.55-1.52 μm) were prepared on both silicon and 316L stainless steel by closed-field unbalanced magnetron sputtering. With the increase of film thickness, the sp^2 content and surface roughness increased, while the compactness decrease in the structure, leading to the dropped hardness and enhanced internal stress. The nano-tribological testing showed the GLC film with the median thickness (1.10 μm) possessed the highest wear resistance due to the combined

advantages in thickness, compactness and hardness. In comparison of the fretting wear testing, both friction coefficient curves exhibited similar initial stable and rising stages corresponding to the negligible wear and dominant abrasive wear respectively, and the distinct trends in the final stage as the different contact stress strongly affected the stability of the in-situ formed transfer films. In addition, the increase of the applied normal loads in nano-tribological testing resulted in the decreased the friction coefficient and wear rate due to the formation of transfer films.

Acknowledgments

The authors of Xiangru Shi and Jian Chen gratefully acknowledge the financial support from the NSFC (#11472080), the NSF of Jiangsu Province (#BK20141336)， the Fundamental Research Funds for the Central Universities, the financial support from the program of China Scholarships Council (No. 201706090126), and the postgraduate training innovation project of Jiangsu Province (KYLX16_0198).

References

[1] Wang Y, Pu J, Wang J, et al. Interlayer design for the graphite-like carbon film with high load-bearing capacity under sliding-friction condition in water[J]. Applied Surface Science, 2014, 311: 816-824.
[2] Field S K, Jarratt M, Teer D G. Tribological properties of graphite-like and diamond-like carbon coatings[J]. Tribology International, 2004, 37(11-12): 949-956.
[3] Bewilogua K, Hofmann D. History of diamond-like carbon films—from first experiments to worldwide applications[J]. Surface and Coatings Technology, 2014, 242: 214-225.
[4] Viana G A, Marques F C. Raman and thermal desorption spectroscopy analyses of amorphous graphite-like carbon films with incorporated xenon[J]. Vacuum, 2015, 112: 17-24.
[5] You T, Niwa O, Chen Z, et al. An amperometric detector formed of highly dispersed Ni nanoparticles embedded in a graphite-like carbon film electrode for sugar determination[J]. Analytical chemistry, 2003, 75(19): 5191-5196.
[6] Chen L, Huang D, Ren S, et al. Preparation of graphite-like carbon nitride nanoflake film with strong fluorescent and electrochemiluminescent activity[J]. Nanoscale, 2013, 5(1): 225-230.
[7] Robertson J. Diamond-like amorphous carbon[J]. Materials Science and Engineering: R: Reports, 2002, 37(4-6): 129-281.
[8] Tribology of diamond-like carbon films: fundamentals and applications[M]. Springer Science & Business Media, 2007.
[9] Wang Y, Li J, Shan L, et al. Tribological performances of the graphite-like carbon films deposited with different target powers in ambient air and distilled water[J]. Tribology International, 2014, 73: 17-24.

[10] Dong D, Jiang B, Li H, et al. Effect of graphite target power density on tribological properties of graphite-like carbon films[J]. Applied Surface Science, 2018, 439: 900-909.
[11] Wang Y, Li H, Ji L, et al. Microstructure, mechanical and tribological properties of graphite-like amorphous carbon films prepared by unbalanced magnetron sputtering[J]. Surface and Coatings Technology, 2011, 205(8-9): 3058-3065.
[12] Huang M, Zhang X, Ke P, et al. Graphite-like carbon films by high power impulse magnetron sputtering[J]. Applied surface science, 2013, 283: 321-326.
[13] A.C. Ferrari, J. Robertson, Raman spectroscopy of amorphous, nanostructured, diamond-like carbon, and nanodiamond, Phil. Trans. R. Soc. Lond. A 362 (2004) 2477-2512.
[14] Ward L, Junge F, Lampka A, et al. The effect of bias voltage and gas pressure on the structure, adhesion and wear behavior of Diamond Like Carbon (DLC) coatings with Si interlayers[J]. Coatings, 2014, 4(2): 214-230.
[15] Guo T, Kong C, Li X, et al. Microstructure and mechanical properties of Ti/Al co-doped DLC films: Dependence on sputtering current, source gas, and substrate bias[J]. Applied Surface Science, 2017, 410: 51-59.
[16] Dai H Y, Zhan C, Du J. Studies on the influence of sputtering power on amorphous carbon films deposited by pulsed unbalanced magnetron sputtering[J]. Optik-International Journal for Light and Electron Optics, 2016, 127(5): 2512-2515.
[17] Manoharan M P, Lee H, Rajagopalan R, et al. Elastic properties of 4–6 nm-thick glassy carbon thin films[J]. Nanoscale research letters, 2010, 5(1): 14.
[18] Wei C, Yen J Y. Effect of film thickness and interlayer on the adhesion strength of diamond like carbon films on different substrates[J]. Diamond and related materials, 2007, 16(4-7): 1325-1330.
[19] Bernoulli D, Wyss A, Raghavan R, et al. Contact damage of hard and brittle thin films on ductile metallic substrates: an analysis of diamond-like carbon on titanium substrates[J]. Journal of materials science, 2015, 50(7): 2779-2787.
[20] Qi J, Chan C Y, Bello I, et al. Film thickness effects on mechanical and tribological properties of nitrogenated diamond-like carbon films[J]. Surface and Coatings Technology, 2001, 145(1-3): 38-43.
[21] Wang D F, Kato K. Coating thickness effect on surface damage mode transitions for an ion beam assisted carbon nitride coating subject to sliding contact with a spherical diamond[J]. Wear, 1998, 223(1-2): 167-172.
[22] Ouyang J H, Sasaki S, Murakami T, et al. Mechanical and unlubricated tribological properties of titanium-containing diamond-like carbon coatings[J]. Wear, 2009, 266(1-2): 96-102.
[23] Stallard J, Mercs D, Jarratt M, et al. A study of the tribological behaviour of three carbon-based coatings, tested in air, water and oil environments at high loads[J]. Surface and Coatings Technology, 2004, 177: 545-551.
[24] Kim D W, Kim K W. Effects of sliding velocity and normal load on friction and wear characteristics of multi-layered diamond-like carbon (DLC) coating prepared by

reactive sputtering[J]. Wear, 2013, 297(1-2): 722-730.
[25] Amanov A, Watabe T, Tsuboi R, et al. Fretting wear and fracture behaviors of Cr-doped and non-doped DLC films deposited on Ti–6al–4V alloy by unbalanced magnetron sputtering[J]. Tribology International, 2013, 62: 49-57.
[26] Du D, Liu D, Ye Z, et al. Fretting wear and fretting fatigue behaviors of diamond-like carbon and graphite-like carbon films deposited on Ti-6Al-4V alloy[J]. Applied Surface Science, 2014, 313: 462-469.
[27] Pharr G M, Oliver W C. Measurement of thin film mechanical properties using nanoindentation[J]. Mrs Bulletin, 1992, 17(7): 28-33.
[28] Cho S J, Lee K R, Eun K Y, et al. Determination of elastic modulus and Poisson's ratio of diamond-like carbon films[J]. Thin solid films, 1999, 341(1-2): 207-210.
[29] Ban M, Hasegawa T. Internal stress reduction by incorporation of silicon in diamond-like carbon films[J]. Surface and Coatings Technology, 2003, 162(1): 1-5.
[30] Kubiak K J, Mathia T G, Fouvry S. Interface roughness effect on friction map under fretting contact conditions[J]. Tribology International, 2010, 43(8): 1500-1507.
[31] Kubiak K J, Liskiewicz T W, Mathia T G. Surface morphology in engineering applications: Influence of roughness on sliding and wear in dry fretting[J]. Tribology International, 2011, 44(11): 1427-1432.
[32] Liskiewicz T, Kubiak K, Comyn T. Nano-indentation mapping of fretting-induced surface layers[J]. Tribology International, 2017, 108: 186-193.
[33] Madsen I C, Scarlett N V Y, Kern A. Description and survey of methodologies for the determination of amorphous content via X-ray powder diffraction[J]. Zeitschrift für Kristallographie Crystalline Materials, 2011, 226(12): 944-955.
[34] Tamor M A, Vassell W C. Raman ‘‘fingerprinting’’of amorphous carbon films[J]. Journal of Applied Physics, 1994, 76(6): 3823-3830.
[35] Schwan J, Ulrich S, Batori V, et al. Raman spectroscopy on amorphous carbon films[J]. Journal of Applied Physics, 1996, 80(1): 440-447.
[36] Ferrari A C, Robertson J. Interpretation of Raman spectra of disordered and amorphous carbon[J]. Physical review B, 2000, 61(20): 14095.
[37] Gradowski M V, Ferrari A C, Ohr R, et al. Resonant Raman characterisation of ultra-thin nano-protective carbon layers for magnetic storage devices[J]. Surface and Coatings Technology, 2003, 174: 246-252.
[38] Kanda K, Yamada N, Okada M, et al. Graphitization of thin films formed by focused-ion-beam chemical-vapor-deposition[J]. Diamond and Related Materials, 2009, 18(2-3): 490-492.
[39] Leyland A, Matthews A. On the significance of the H/E ratio in wear control: a nanocomposite coating approach to optimised tribological behaviour[J]. Wear, 2000, 246(1-2): 1-11.
[40] Chen J, Li H, Beake B D. Load sensitivity in repetitive nano-impact testing of TiN and AlTiN coatings[J]. Surface and Coatings Technology, 2016, 308: 289-297.
[41] Du D, Liu D, Ye Z, et al. Fretting wear and fretting fatigue behaviors of diamond-like carbon and graphite-like carbon films deposited on Ti-6Al-4V alloy[J]. Applied

Surface Science, 2014, 313: 462-469.
[42] Hwang M S, Lee C. Effects of oxygen and nitrogen addition on the optical properties of diamond-like carbon films[J]. Materials Science & Engineering B, 2000, 75(1):24-28.
[43] Lifshitz Y, Kasi S R, Rabalais J W, et al. Subplantation model for film growth from hyperthermal species[J]. Physical Review B, 1990, 41(15): 10468.
[44] Lifshitz Y, Kasi S R, Rabalais J W. Subplantation model for film growth from hyperthermal species: Application to diamond[J]. Physical review letters, 1989, 62(11): 1290.
[45] Robertson J. Deposition mechanisms for promoting sp3 bonding in diamond-like carbon[J]. Diamond and related materials, 1993, 2(5-7): 984-989.
[46] Dai H Y, Cheng X R, Wang C F, et al. Structural, optical and electrical properties of amorphous carbon films deposited by pulsed unbalanced magnetron sputtering[J]. Optik-International Journal for Light and Electron Optics, 2015, 126(7-8): 861-864.
[47] P. Wang, X. Wang, Y. Chen, G. Zhang, W. Liu, J. Zhang, The effect of appliednegative bias voltage on the structure of Ti-doped aC: H films deposited byFCVA, Applied Surface Science 253 (2007) 3722.
[48] M. Siegal, D. Tallant, L. Martinez-Miranda, J. Barbour, R. Simpson, D. Overmyer, Phys. Rev. B 61 (2000) 10451
[49] Chowdhury S, Laugier M T, Rahman I Z. Effects of substrate temperature on bonding structure and mechanical properties of amorphous carbon films[J]. Thin Solid Films, 2004, 447: 174-180.
[50] Chen J, Wang Y, Li H, et al. Microstructure, morphology and properties of titanium containing graphite-like carbon films deposited by unbalanced magnetron sputtering[J]. Tribology Letters, 2013, 49(1): 47-59.
[51] Baptista D L, Zawislak F C. Hard and sp2-rich amorphous carbon structure formed by ion beam irradiation of fullerene, aC and polymeric aC: H films[J]. Diamond and related materials, 2004, 13(10): 1791-1801.
[52] Fallon P J, Veerasamy V S, Davis C A, et al. Properties of filtered-ion-beam-deposited diamondlike carbon as a function of ion energy[J]. Physical Review B, 1993, 48(7): 4777.
[53] Wang P, Wang X, Xu T, et al. Comparing internal stress in diamond-like carbon films with different structure[J]. Thin Solid Films, 2007, 515(17): 6899-6903.
[54] L.F. Binetti, G. Capote, L.V. Santos, E.J. Corat, V.J. Trava-Airoldi, Adhesion studies of diamond-like carbon films deposited on Ti6Al4V substrate with a silicon interlayer, Thin Solid Films 515 (2006) 375–379.
[55] C. Wei, J.Y. Yen, Effect of film thickness and interlayer on the adhesion strength of diamond like carbon films on different substrates, Diamond Relat. Mater. 16 (2007) 1325–1330.
[56] Holmberg K, Ronkainen H, Laukkanen A, et al. Friction and wear of coated surfaces—scales, modelling and simulation of tribomechanisms[J]. Surface and Coatings Technology, 2007, 202(4-7): 1034-1049.

[57] Sanchez-Lopez J C, Erdemir A, Donnet C, et al. Friction-induced structural transformations of diamondlike carbon coatings under various atmospheres[J]. Surface and Coatings Technology, 2003, 163: 444-450.
[58] Charitidis C A. Nanomechanical and nanotribological properties of carbon-based thin films: a review[J]. International Journal of Refractory Metals and Hard Materials, 2010, 28(1): 51-70.

Supporting Information

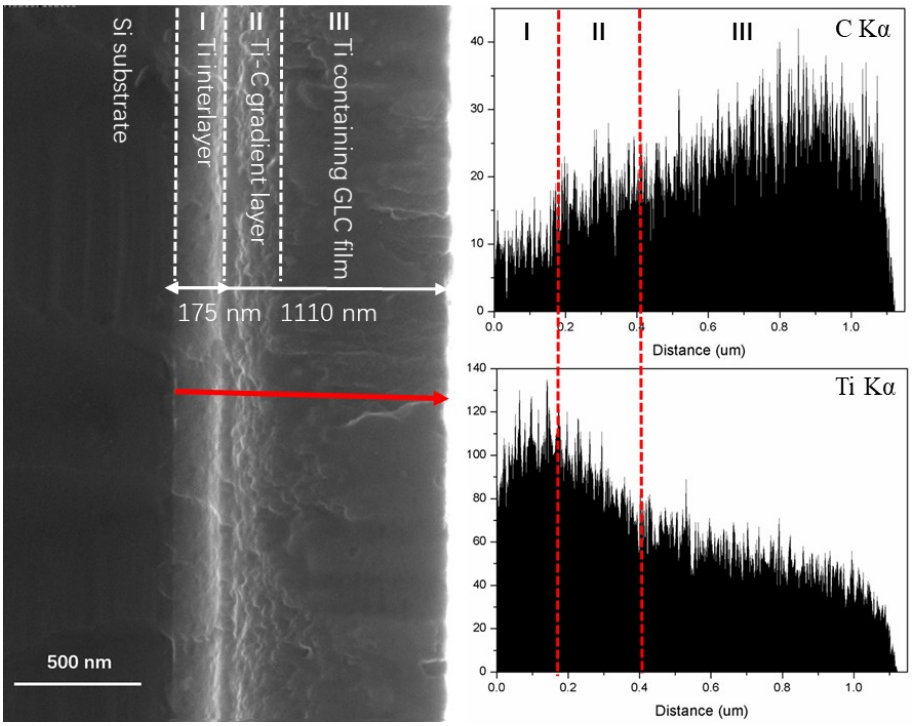

Figure S1. Cross-sectional morphology and EDX spectra of 1h GLC sample.

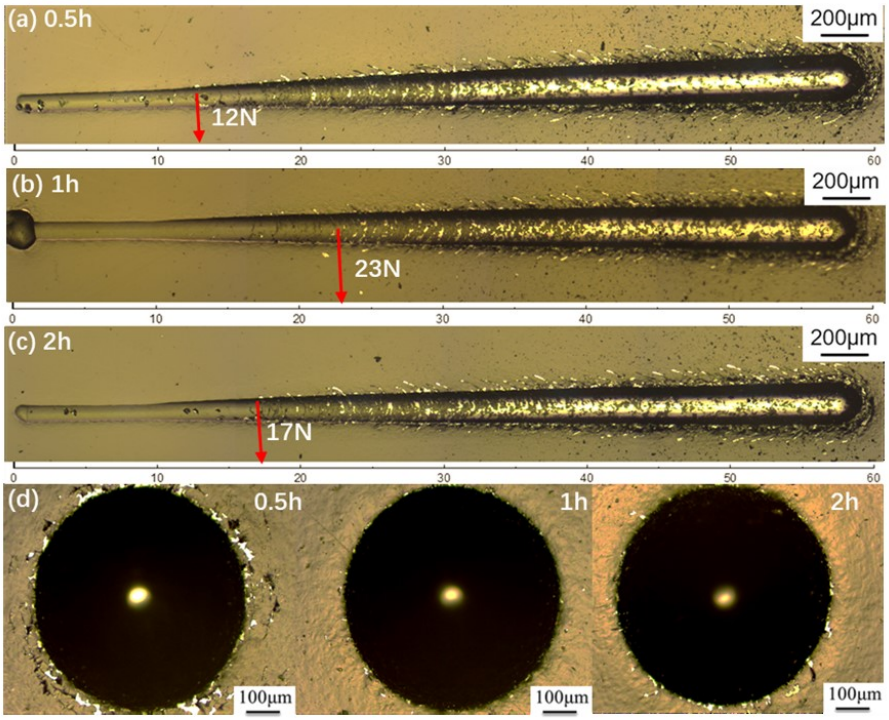

Figure S2. Optical images of scratch traces on films (a) 0.5h, (b) 1h, (c) 2h, and (d) morphologies of Rockwell indentation for GLC films.

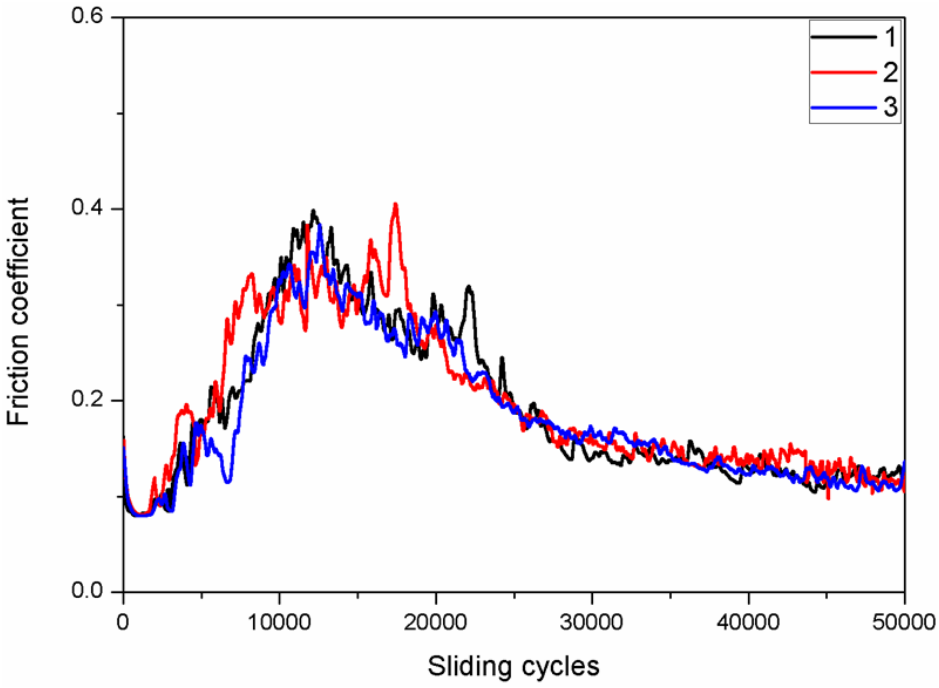

Figure S3. Three repeated friction coefficient curves of 1h GLC films as a function of sliding cycles at a normal load of 1000mN for nanotribological tests.